Journal of Hazardous Materials 186 (2011) 1672–1680

Contents lists available at ScienceDirect

Journal of Hazardous Materials

journal homepage: www.elsevier.com/locate/jhazmat

Preparation of novel nano-adsorbent based on organic–inorganic hybrid and their adsorption for heavy metals and organic pollutants presented in water environment

Xinliang Jin, Cui Yu, Yanfeng Li*, Yongxin Qi, Liuqing Yang, Guanghui Zhao, Huaiyuan Hu

College of Chemistry and Chemical Engineering, State Key Laboratory of Applied Organic Chemistry, Institute of Biochemical Engineering & Environmental Technology, Lanzhou University, Lanzhou 730000, PR China

ARTICLE INFO

Article history:
Received 23 September 2010
Received in revised form 9 December 2010
Accepted 13 December 2010
Available online 21 December 2010

Keywords:
Organic–inorganic hybrid
Nano-adsorbent
Pb^{2+}
Phenol
Adsorption

ABSTRACT

The nanocomposites based on organic–inorganic hybrid have been attracting much attention due to their potential applications used as new type of functional materials, such as colloidal stabilizers, electro-optical devices, and nanocomposites materials. The organic–inorganic hybrid of poly(acrylic acid-acrylonitrile)/attapulgite, P(A-N)/AT nanocomposites, were prepared by using *in situ* polymerization and composition of acrylic acid (AA) and acrylonitrile (AN) onto modified attapulgite (AT) nanoparticles. The resulting P(A-N)/AT nanocomposites were transformed into novel nano-adsorbent of poly(acrylic acid-acryloamidoxime)/attapulgite by further functionalization, i.e. P(A-O)/AT nano-adsorbent. The adsorption properties of P(A-O)/AT toward metal ions were determined, and the results indicated that the adsorbents with nanocomposite structure held a good of selectivity to Pb^{2+} among numerous metal ions. The maximum removal capacity of Pb^{2+} was up to 109.9 mg/g and it is notable to see that the adsorption removal of P(A-O)/AT nano-adsorbent for Pb^{2+} could achieve more than 96.6% when the initial concentration of Pb^{2+} was 120.0 mg/l. The kinetics, isotherm models, and conductivity were introduced to study the adsorption mechanism of P(A-O)/AT for Pb^{2+} and it was concluded that it could be chemisorptions process and the best coordination form took place when AO:AA:Pb^{2+} = 1:1:1. In addition, after simply treated with CTAB, P(A-O)/AT nano-adsorbent showed better adsorption properties for phenol than the same kinds of materials.

1. Introduction

Industrial wastewater contains numerous toxic organic and inorganic contaminations, such as heavy metals and phenolic compounds. The toxic heavy metal and phenols discharged into water environment would lead to a serious pollution problem affecting water quality. Especially, the heavy-metal ions from plating plants, mining, metal finishing, welding, and alloys manufacturing have already endangered the sustainable development of human society [1–3]. On the other hand, phenol contaminants in wastewaters generated from petroleum, coal conversion, and phenol producing industries are considered one of the priority pollutants in wastewater, because they were harmful to organisms even at low concentrations [4,5], so that they had been classified as hazardous pollutants based on their potential toxicity to human health. Therefore, Environmental Protection Agency (EPA) regulations call for lowering phenol content in wastewater to less than 1 ppm [6].

There are many methods to remove metal ions and phenol from aqueous solutions, such as adsorption, ion exchange, chemical precipitation, and membrane processes [7–12]. Adsorption is the most popular way in which activated carbon or ion exchange resins are usually applied. Although they have the advantage of high adsorption capacity for heavy metals and phenolic compounds [13–16], high cost usually limits their application widely. There have been attempts to utilize low cost, naturally occurring adsorbents to remove contaminants from wastewater. In recent years, a number of adsorbent materials such as tea factory waste [17], phenolated wood resin [18], kaolinite [19], zeolites [20], and modified jute [21] have been employed in removal of heavy metal and organic pollutants removal from wastewaters. The obvious advantage of these adsorption methods was the lower costs involved. However, new adsorbents which were locally available and had high adsorption capacity were still required [22–24].

Hydrophilic polymers have been widely used in removal of toxic pollutants from aqueous solution for environmental control [25,26]. Among the potential adsorbents for removal of heavy metal ions such as Ag^{+}, Pb^{2+} [27,28] and phenol [29,7,30], polymeric adsorbents with high surface area and pore structure have

* Corresponding author. Tel.: +86 931 8912528; fax: +86 931 8912113.
E-mail address: liyf@lzu.edu.cn (Y. Li).

0304-3894/$ – see front matter © 2010 Elsevier B.V. All rights reserved.
doi:10.1016/j.jhazmat.2010.12.057

proved to be the promising candidates. Liu's group reported that the capable removal of Pb^{2+} from aqueous solutions by using synthetic polymer P(AO/AN/MA) which could achieve adsorption capacity of 4.28 mmol/g at 25 °C [31]. Polymers which could selectively adsorb metal ions should consist of two monomer groups, each having a different role. One functional group forms a complex with the target and the other allows the polymers to stretch and shrink reversibly in response to environmental change. Generally, amidoxime (AO) and carboxylic groups (AA) were chosen as the functional groups [32–34]. So that, utilizing the similar strategy to construct organic–inorganic hybrid material would be very interesting.

The goal of the present work was to investigate the adsorption potential of the organic–inorganic hybrid nano-adsorbent for removal of Pb^{2+} and phenol presented in individual solutions. In this paper, we synthesized the organic–inorganic hybrid nano-adsorbent P(A-O)/AT and studied the adsorption selectivity to Pb^{2+} and phenols. The kinetics, isotherm models, and conductivity were introduced to study lead adsorption mechanism. Moreover, the effect of pH, contact time on phenol adsorption capacity of P(A-O)/AT was studied, and kinetics and factors controlling the adsorption process were also researched.

2. Materials and methods

2.1. Materials

Attapulgite (AT) with the average diameter of 325 mesh, was provided by Gansu AT Co. Ltd., Gansu, China. It was dried in a desiccator at 50 °C, and then stored in the desiccator for subsequent analyses. γ-Methacryloxypropyl trimethoxy silane (KH-570) was supported by Wu Han University. Acrylic acid (AA) and acrylonitrile (AN) provided by Sinopharm Chemical Regent Co. Ltd. were distilled just before polymerization. 2,2′-Azo-bisiso-butyronitrile (AIBN) was provided by Shanghai Chemical Co. All other chemicals of analytical grade were used as received without any further purification.

2.2. Preparation of KH-570-modified AT nanocomposites

The coupling reagent KH-570 was used to introduce ethylene groups onto the AT surface before the graft polymerization was initiated. Typically, 2.5 g of AT were dispersed in 100 ml of ethanol by sonication for about 1 h, then 12 ml of $NH_3{\cdot}H_2O$ was added and dispersed with ultrasonic agitation to homogenize for 10 min. Under continuous mechanical stirring, 6.0 ml of KH-570 was added to the reaction mixture. The reaction was allowed to proceed at 55 °C for 8 h under continuous stirring under N_2 atmosphere. After that, the resultant products were separated by centrifugation and were washed with ethanol and distilled water until neutral. The KH-570-modified AT was dried in a desiccator at 50 °C.

2.3. Synthesis of P(A-N)/AT nanocomposites

The grafted polymerization was conducted under various reaction conditions. In a typical protocol, 0.5 g of KH-570-modified AT nanocomposites, 3.0 g of AN, 1.0 g of AA, 25 ml of DMF, and 25 ml of deionized water were put into a three-necked-flask and vibrated with ultrasonic for 30 min to be dispersed uniformly. Then 0.10 g of AIBN was added and the flask was placed in an oil bath at 80 °C, mechanically stirred at 300 rpm under nitrogen. The graft polymerization was undergone at 80 °C for 6 h. N_2 was bubbled throughout the polymerizing period. After that, the products were separated by centrifugation and were thoroughly washed with DMF, distilled water, and ethanol several times, then dried at room temperature under vacuum for 12 h.

2.4. Preparation of P(A-O)/AT nano-adsorbent

0.50 g of $NH_2OH{\cdot}HCl$, 4.80 g of Na_2CO_3, 8.1 ml deionized water, and 50 ml of ethanol were added into a reactor equipped with a magnetic stirrer and a reflux condensator, the mixture was stirred for 0.5 h. After that, 0.50 g of P(A-N)/AT nanocomposites were added to this mixture. The reaction was performed for two steps, 4 h at 40 °C and then 10 h at 85 °C under stirring. The modified nanocomposites were washed thoroughly with a large amount of distilled water then extracted in ethanol for 12 h, dried at 50 °C under vacuum for 12 h.

2.5. Modification of P(A-O)/AT with CTAB

0.30 g of P(A-O)/AT nanocomposites were added to 30 ml of 0.008 mol/l CTAB solution before the mixture was sonicated for 0.5 h. Next, the particles were separated, washed, dried, and crushed.

2.6. Adsorption experiments

All the adsorption experiments were carried out at adsorbent dosages of 2 g/l and shaking in a shaking thermostatic bath (SHZ-B, China) at 140 rpm at 25 °C for a given time. After adsorption, the solid and liquid phases were separated by centrifugation. Pb^{2+} concentrations in the solution samples were determined by atomic absorption spectrophotometer (AAS).

Pb^{2+} adsorption isotherms and the effects of the initial concentration were studied in the range of 100–700 ppm. The effects of pH were studied in the range of 1.0–6.0, with 0.1 mol/l HNO_3 and NaOH used as pH controls. The effects of contact time on adsorption were determined in the range of 0–960 min.

The pH effects of phenol adsorption were studied in the range of 1.0–13.0, with 0.1 mol/l HCl and NaOH used as pH controls. Contact time on adsorption was determined in the range of 0–96 h.

2.7. Characterization

The product structures were characterized using a Nicolet Magna-IR 550 spectrophotometer between 4000 and 450 cm^{-1}. Conductivities were measured with a DDS-307 conductivity meter. A Hanna ammonia ion specific meter (HI 93733) was used to measure the ammonia concentration in the solution before and after phenol adsorption in the mechanism study. The concentrations of ions in solution were determined by a GBC Avanta A 5450 atomic absorption spectrophotometer (AAS). The pH of solutions was determined using a HANNA pH meter. Specific surface area was determined by the BET method based N_2 adsorption on a Autosorb-1 at 76 K. The XPS spectra of P(A-O)/AT before and after Pb^{2+} adsorption were recorded by an X-ray photoelectron spectrometer (VG Scientific Escalab 210-UK) equipped with a twin anode (Mg Kα/Al Kα) source. All binding energies (BEs) were referenced to the C 1s hydrocarbon peak at 285.0 eV.

3. Results and discussion

3.1. Structure of P(A-O)/AT nano-adsorbent

The preparation of P(A-O)/AT was shown schematically in Fig. 1. Fig. 2 shows the FTIR spectra of AT, KH-570-modified AT, P(A-N)/AT, P(A-O)/AT, and CTAB-modified P(A-O)/AT. The new peaks at 1705 and 1455 cm^{-1} for KH-570-modified AT (Fig. 2b) were usually representative of the carboxyl group ($-COO^-$) and –C=C

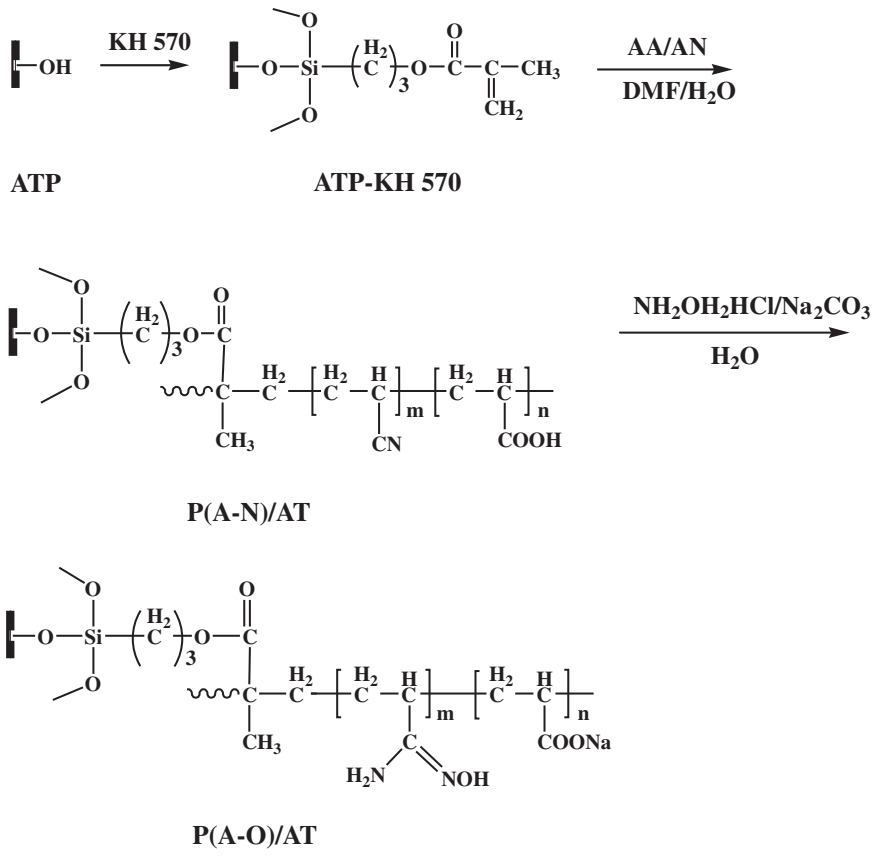

Fig. 1. Scheme for the preparation procedure to P(A-O)/AT.

group, suggesting that the silane coupling agent reacted successfully with the –OH groups. Bands of AN and AA units were observed for unmodified copolymers: 2243 cm^{-1} (–C≡N); 1734 cm^{-1} (–C=O) (Fig. 2c); the disappearance of a band at 2243 cm^{-1} related to the–C≡N group on the modified copolymer spectrum suggested that the modifications of cyano groups were almost complete. The increase of the absorption bands at 1618 cm^{-1} were attributed to –C=N– of the AO groups (Fig. 2d), and the appearance of a band at 1575 cm^{-1} was attributed to the carboxylate in the polymer. In addition, the increase in the absorption bands around 3340–3650 cm^{-1} compared to FTIR spectrum of the unmodified copolymers (Fig. 2c) indicated the presence of –OH bonds that belong to AO groups. These changes indicated that the modification reaction was successfully done. To compare the differences among the P(A-O)/AT and CTAB-modified P(A-O)/AT, the FTIR spectra of the two kinds of nanocomposites were shown in Fig. 2d and e. The bands at 2700–3000 cm^{-1} of CTAB-modified P(A-O)/AT (Fig. 2e) were related to the stretching vibrations of C–H groups.

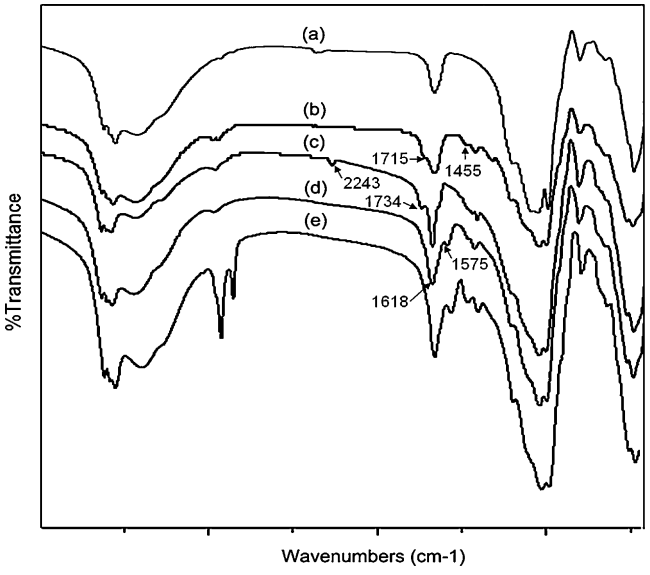

Fig. 2. FTIR spectra of (a) ATP; (b) KH-570-modified ATP; (c) P(A-N)/AT; (d) P(A-O)/AT; (e) CTAB-modified P(A-O)/AT.

3.2. Adsorption of nano-adsorbent for Pb^{2+}

Adsorption experiment revealed that the nano-adsorbent altered its selectivity to Pb^{2+} among the metal ions. Commonly coexistent metal ions, e.g., Co^{2+}, Zn^{2+}, Cd^{2+}, Ag^{+}, Ba^{2+}, Hg^{2+}, and Ca^{2+}, displayed little interference for the nano-adsorbent. The experiment data showed that the material display excellent adsorption characteristic for Pb^{2+}.

3.2.1. Effect of initial pH

The pH value played a very important role in the use of nano-adsorbent as supports in the metal ion adsorption process. This was partly for the reason that hydrogen ions themselves were strongly competing with metal ions. It was not only affecting the electronic status of the pendant functional groups, for instance protonation/deprotonation of the basic groups or dissociation/association of acidic groups, but it might also alter the oxidation form of the metal ions present in the medium [35]. Fig. 3 shows the effect of pH on the adsorption of Pb^{2+} onto P(A-N)/AT and P(A-O)/AT. As expected, the higher the acidic condition, the lower adsorption of metal ions, this might be for the reason of the protonation of the

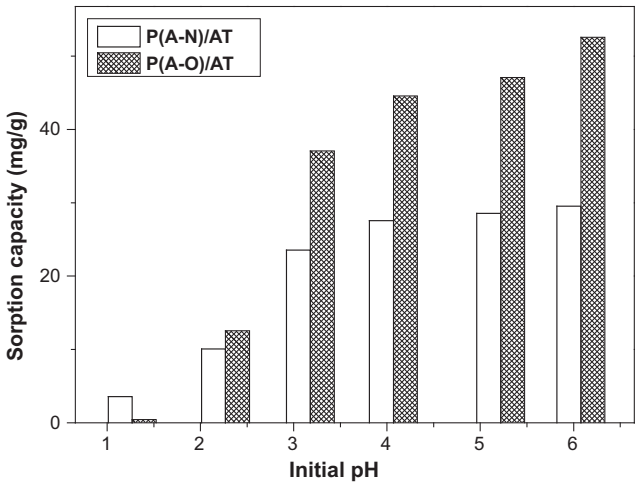

Fig. 3. Effect of initial pH on the adsorption of Pb^{2+}.

amino groups at the acidic conditions. Moreover, there was a competitive adsorption between H^+ ions and Pb^{2+} in the solution. As shown in Fig. 12, a significant increase in the concentration of H^+ led to the adsorption balance moving to the left, which was not conducive to adsorption because of bad competition. In reverse the adsorption balance moved to the right, which resulted in excellent metal ions adsorption. A considerable increase in the adsorption occurred at pH = 5–6 and the maximum amount of Pb^{2+} adsorption was observed at these pH values. At higher pH values, metal precipitation took place and the adsorbent was deteriorated with the accumulation of metal ions onto surfaces [36].

3.2.2. Adsorption kinetics

The relationship between reaction time and sorption amounts at the initial Pb^{2+} concentrations of 120 mg/l was presented in Fig. 4. The results showed the adsorption of Pb^{2+} onto P(A-N)/AT, P(A-O)/AT was very rapid with increase in contact time from 0 to 60 min, and sorption equilibration was achieved by 120 min and 480 min, respectively, followed by a constant adsorption rate with further shaking time. The initial rapid step of Pb^{2+} sorption might be due to the surface physical sorption because of large surface area, around 108.3379 m^2/g, obtained from BET test and chemical reactive sorption because of a facilely immediate interaction between Pb^{2+} and the reactive groups (i.e. $-NH_2$, –OH, $-COO^-$)

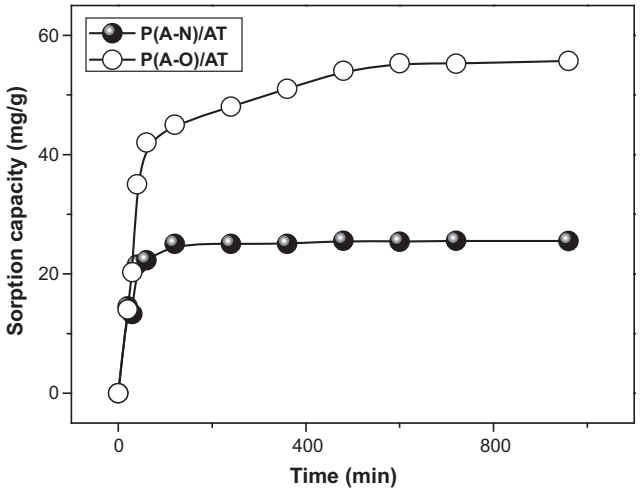

Fig. 4. Effect of contact time on the adsorption of Pb^{2+}.

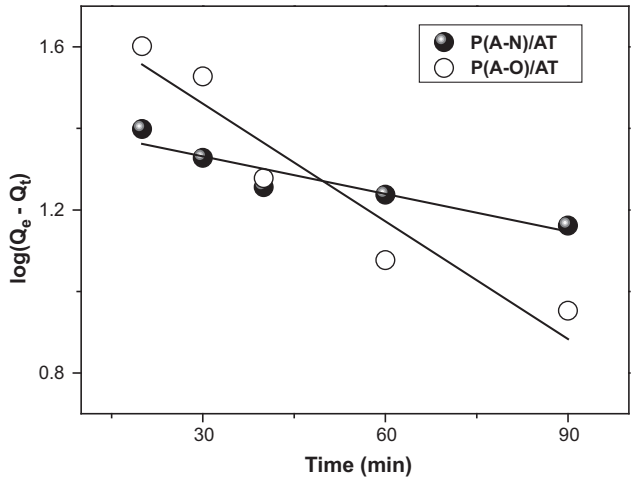

Fig. 5. The pseudo-first-order kinetics for the adsorption of Pb^{2+} onto P(A-N)/AT and P(A-O)/AT.

Table 1
Parameters of kinetic models of Pb^{2+} adsorption onto P(A-N)/AT and P(A-O)/AT.

Samples	Pseudo-first-order			Pseudo-second-order		
	Q_{e1} (mg/g)	K_1 (min^{-1})	R_1^2	Q_{e2} (mg/g)	K_2 (g/mg min)	R_2^2
P(A-N)/AT	26.53	0.0071	0.8915	25.90	41.5×10^{-4}	0.9985
P(A-O)/AT	56.13	0.0221	0.9111	57.47	4.72×10^{-4}	0.9803

[37,38] on the surface of the nano-adsorbent (this mechanism would be explained in detail in Section 3.2.4). However, the subsequent slow step might be attributable to the reactive sorption within the polymer chain segments [39]. Besides, the Pb^{2+} adhered on the surface of the nano-adsorbent would further hamper the diffusion of other Pb^{2+}, resulting in a rather long time to reach the equilibrium. The pseudo-first-order and pseudo-second-order kinetic equations were employed to analyze the sorption kinetics of Pb^{2+} onto the hybrid materials. The curves of log(Qe – Qt) versus t and t/Qt versus t based on the experiment data were shown in Figs. 5 and 6. From the corresponding parameters summarized in Table 1, it was observed that the kinetic behavior of Pb^{2+} sorption onto the particles was more appropriately described by the pseudo-second-order model developed based on the assumption that the

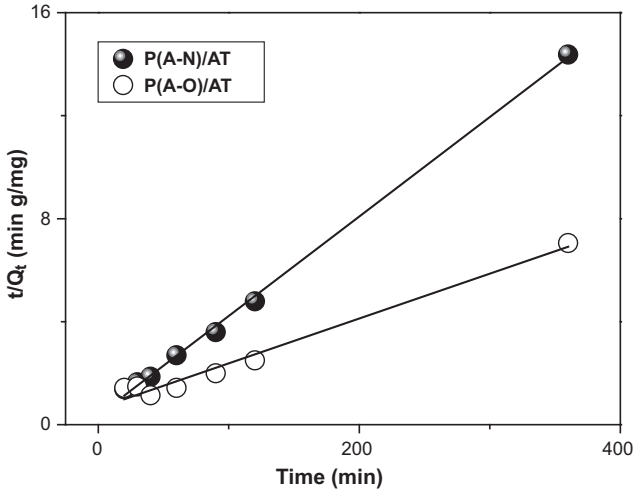

Fig. 6. The pseudo-second-order kinetics for the adsorption of Pb^{2+} onto P(A-N)/AT and P(A-O)/AT.

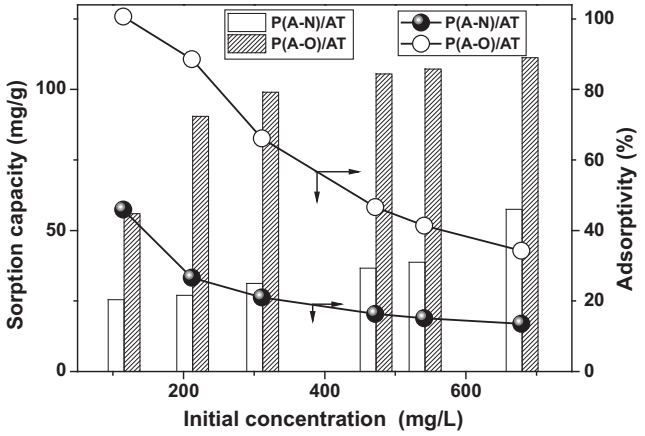

Fig. 7. Effect of initial Pb^{2+} ions concentration on the adsorption.

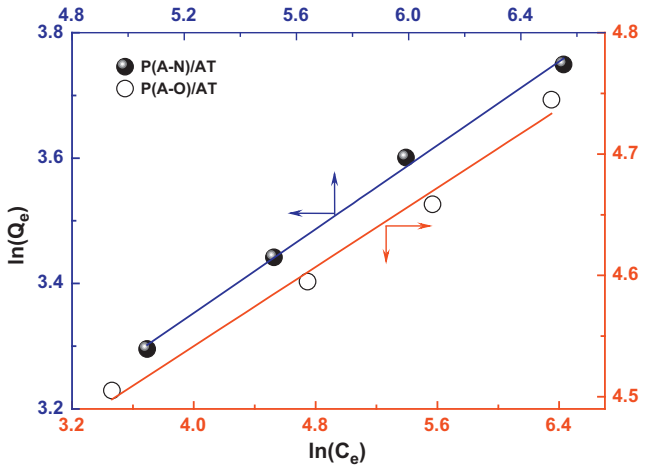

Fig. 8. Freundlich isotherms of Pb^{2+} adsorbed onto P(A-N)/AT and P(A-O)/AT.

determining rate step might be chemisorption promoted by covalent forces through the electron exchange or valency forces through electrons sharing between sorbent and sorbate, indicating that the behavior of Pb^{2+} sorption on P(A-N)/AT and P(A-O)/AT was in agreement with chemical adsorption, which was the rate-controlling step [40,41]. Interestingly, Pb^{2+} adsorption onto P(A-N)/AT was much faster, the amount of Pb^{2+} adsorbed per unit weight of adsorbent was much smaller than that onto P(A-O)/AT, indicating that the amidoxime groups grafted onto the surface of AT could enhance the adsorption of Pb^{2+} greatly.

3.2.3. Adsorption isotherms

The effect of the initial Pb^{2+} concentration on sorption of Pb^{2+} onto the P(A-N)/AT and P(A-O)/AT was shown in Fig. 7. The Pb^{2+} adsorbance rose significantly with an increase in Pb^{2+} concentration, whereas the adsorptivity declined. At a lower initial Pb^{2+} concentration, especially in the range of 0–120 mg/l, abundant active groups on the surface of nano-adsorbent could react with Pb^{2+}, resulting in a significantly increased adsorbance of Pb^{2+}. Then the sorption process gradually became slow with increasing initial Pb^{2+} concentration. The highest adsorptivity achieved in this study was 96.64% at the concentration of 120 mg/l. That was to say, almost all Pb^{2+} would be adsorbed onto the nano-adsorbent if the initial Pb^{2+} concentration was below 120 mg/l. It could be seen that the amounts of Pb^{2+} adsorbed onto P(A-O)/AT were much more than the amounts adsorbed by P(A-N)/AT, since strong adsorption groups of amide oxime were introduced to the P(A-O)/AT nano-adsorbent.

The isotherms revealed that the adsorption capacity increased with equilibrium concentration. The data in Fig. 7 was analyzed with Freundlich and Langmuir equations, respectively. The modeled quantitative relationship between Pb^{2+} concentration and the sorption process was shown in Figs. 8 and 9 and the calculated correlation coefficients and standard deviations were listed in Table 2. It could be seen that the sorption isotherm behavior of Pb^{2+} onto the nano-adsorbent did not fit the Langmuir model very well with the correlation coefficients of less than Freundlich model. This might result from the chemisorption processes of Pb^{2+} onto P(A-N)/AT, and P(A-O)/AT.

Table 2
The Langmuir and Freundlich equations, the values of parameters and correlation coefficients.

Samples	Langmuir			Freundlich		
	Q_{m1} (mg/g)	K_L (l/mg)	R_1^2	K (mg/g) $(l/mg)^{1/n}$	n	R_2^2
P(A-N)/AT	57.47	0.0053	0.9399	5.707	3.248	0.9969
P(A-O)/AT	109.89	0.1360	0.8397	67.73	12.27	0.9881

3.2.4. Adsorption mechanism

3.2.4.1. XPS spectra. To provide evidence for the adsorption mechanism, XPS analyses were conducted for P(A-O)/AT before and after Pb^{2+} adsorption, XPS were employed. The changes in surface C 1s, Si 2s, Si 2p, Pb 4f, Na 1s, Na KLL O 1s and N 1s element contents were demonstrated by XPS surface analyses of P(A-O)/AT before and after Pb^{2+} adsorption (Fig. 10). It can be clearly seen that new peaks for Na 1 s and Na KLL before Pb^{2+} adsorption and a new peak for Pb 4f became visible after Pb^{2+} adsorption for P(A-O)/AT.

It is showed in Fig. 11 that, before Pb^{2+} adsorption, there were two peaks in the N 1s spectrum at BEs of about 399.76 eV and 401.49 eV (Fig. 11a). The 399.76 eV peak could be attributed to the nitrogen atoms in –C(**N**H_2)=**N**-OH groups. The other peak at a BE of 401.49 eV was due to the formation of R-NH_2Na^+ complexes in the P(A-O)/AT synthesis. In the complexes, a lone pair of electrons in the nitrogen atom was donated to the shared bond between N and Na^+. As a consequence, the electron cloud density of the nitrogen atom was reduced, resulting in a higher BE peak observed [42]. After Pb^{2+} adsorption, three peaks appeared in the N 1s spectrum (Fig. 11b). The new peak at a BE of 401.52 eV may be due to the formation of R-NH_2Pb^{2+} complexes for Pb^{2+} taking the place of Na^+, but the intensity of this peak was larger than the former 401.49 eV peak, indicating the increased amount of metal–NH_2 complex. The new peak (N*) at a BE of 397.26 eV indicates an increase in electron den-

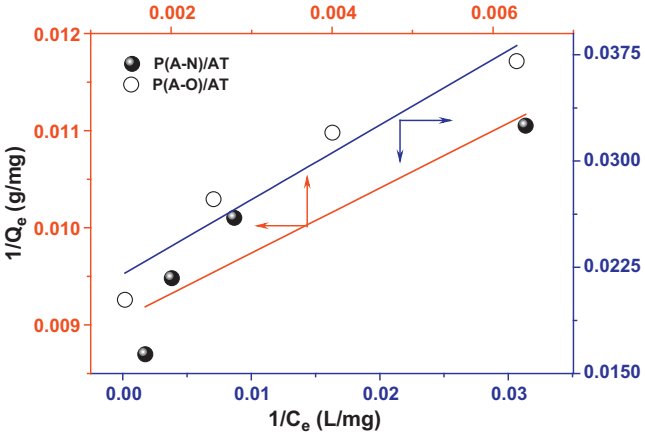

Fig. 9. Langmuir isotherms of Pb^{2+} adsorbed onto P(A-N)/AT and P(A-O)/AT.

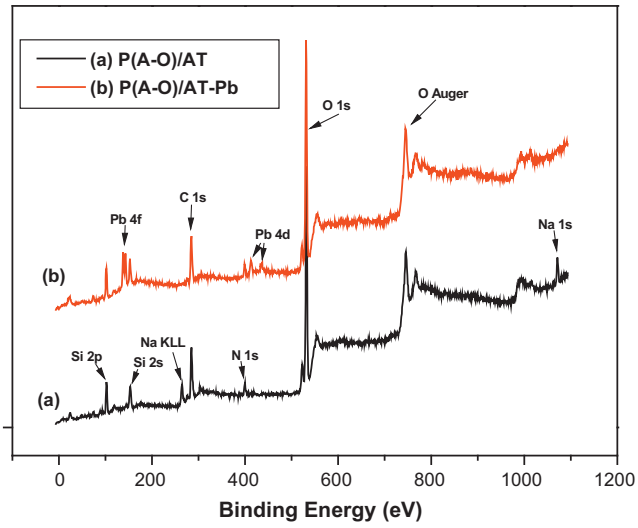

Fig. 10. Typical XPS spectra of P(A-O)/AT: (a) before Pb^{2+} adsorption; (b) after Pb^{2+} adsorption.

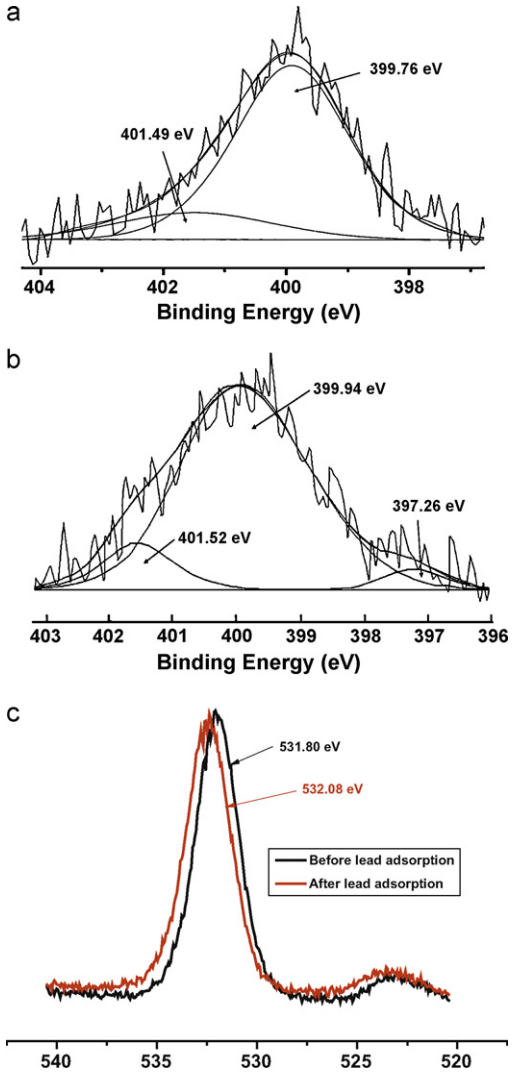

Fig. 11. XPS N 1s spectra of P(A-O)/AT: (a) before Pb^{2+} adsorption; (b) after Pb^{2+} adsorption. (c) O 1s before and after Pb^{2+} adsorption.

Table 3
The samples of $Pb(NO_3)_2$, Ac and AO (with equivalent ratio of AA and AO).

Samples	1	2	3	4	5	6	7	8	9
$V_{(Pb(NO_3)_2)}$ (ml)	8	7	6	5	4	3	2	1	0
$V_{(Ac)}$ (ml)	0	0.5	1	1.5	2	2.5	3	3.5	4
$V_{(AO)}$ (ml)	0	0.5	1	1.5	2	2.5	3	3.5	4
κ (S/cm)	4.64	4.8	5.54	7.3	8.93	7.05	5.87	3.02	1.06

$C_{Ac} = C_{AO} = 0.02$ mol/l, $C_{Pb(NO_3)_2} = 0.01$ mol/l, pH = 4.50, $T = 298$ K, contact time = 24 h.
$\Lambda_m^{\infty}(1/2\ Pb^{2+}) = 7.0 \times 10^{-3}\ S\,m^2\,mol^{-1}$, $\Lambda_m^{\infty}(H^+) = 3.498 \times 10^{-2}\ S\,m^2\,mol^{-1}$.

sity for the nitrogen atoms. Further increase in lead loading results in the shifting of the new N 1s peak component (N*) to a lower BE and an increase in relative intensity of the N* peak component. As mentioned above, the XPS results support an adsorption mechanism of covalent bonds formed between Pb^{2+} and amide groups. The changes in the N 1s spectral line shapes indicate that strong interactions must have occurred between the lead atoms and the nitrogen atoms of the amidoxime groups on the P(A-O)/AT surface [43]. Moreover, the BE of O 1s electron of P(A-O)/AT-Pb (531.80 eV) are found to be 0.28 eV(Fig. 11c), lower than that of O 1s electron in the adsorbent P(A-O)/AT (532.08 eV). However, the peak O 1s almost kept the same shape before and after lead adsorption, which may be caused by the similarity bonding mode between $–COO^-Na^+$ before lead adsorption and $–COO^-Pb^{2+}$ after adsorption.

3.2.4.2. Conductivity test. In order to study the mechanism of complexation relationship between ligand groups and metal ions, both of the hydroxyacetamidine—amidoxime group (AO) and acetic acid—carboxylic group (AA) should be taken into consideration as P(A-O)/AT mainly contains the groups as mentioned above. Fig. 12 represented the expected mechanism in the adsorption of Pb^{2+} by these two functional groups. Hydroxyacetamidine (amidoxime group) was prepared according to Ref. [44].

Generally, the conductivity ($k = \Lambda_m c$) of a solution depends on the concentration of free ions (c) and the molar conductivity (Λ_m). As described in the formula in Fig. 12, the concentration of H^+ increases as the amidoxime and carboxylic groups coordinate metal ions widely causing larger conductivity value. In either these cases, altering the ratio of metal ion and ligand, or the proportion of different ligands (the amidoxime and carboxylic groups) would change the coordination effect. Appropriate ratio can lead to the sufficient coordination as described in Fig. 12 with the maximum value of conductivity. The result of conductivity experiment illustrated that the coordination ratio of metal ion and ligands concentration was 1:1 (Fig. 13, Table 3), the conductivity reached maximum, that was, the best coordination form. As shown in Fig. 14 and Table 4, the conductivity reached maximum when AO:AA = 1:1. It was concluded that form of coordination was consistent with the expected form and the best ratio for the coordination was $AO:AA:Pb^{2+} = 1:1:1$, and it mainly existed as the form of complexes (a) (Fig. 12).

3.3. Adsorption of modified nano-adsorbent for phenol

The adsorption selectivity of CTAB-modified P(A-O)/AT to organic molecules was conducted among toluene, phenol,

Table 4
The samples of $Pb(NO_3)_2$, Ac and AO (with different ratio of AA and AO).

Samples	1	2	3	4	5	6	7	8	9
$V_{(Pb(NO_3)_2)}$ (ml)	4	4	4	4	4	4	4	4	4
$V_{(Ac)}$ (ml)	4	3.5	3	2.5	2	1.5	1	0.5	0
$V_{(AO)}$ (ml)	0	0.5	1	1.5	2	2.5	3	3.5	4
κ (S/cm)	2.70	3.6	5.21	7.03	8.61	6.05	5.55	3.61	1.02

$C_{Ac} = C_{AO} = 0.02$ mol/l, $C_{Pb(NO_3)_2} = 0.01$ mol/l, pH = 4.50, $T = 298$ K, contact time = 24 h.
$\Lambda_m^{\infty}(1/2\ Pb^{2+}) = 7.0 \times 10^{-3}\ S\,m^2\,mol^{-1}$, $\Lambda_m^{\infty}(H^+) = 3.498 \times 10^{-2}\ S\,m^2\,mol^{-1}$.

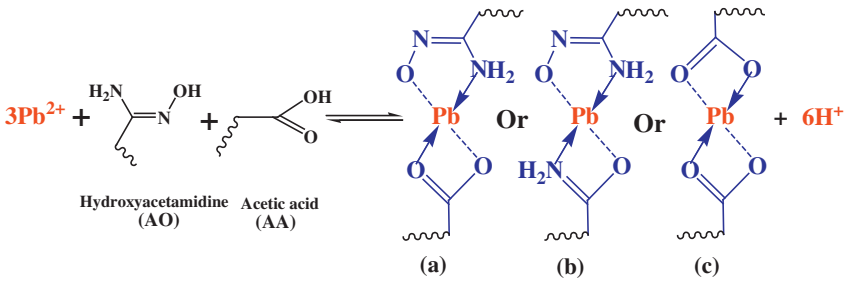

Fig. 12. Proposed schematic diagram for the complex formation between Pb^{2+} ions, AO and AA.

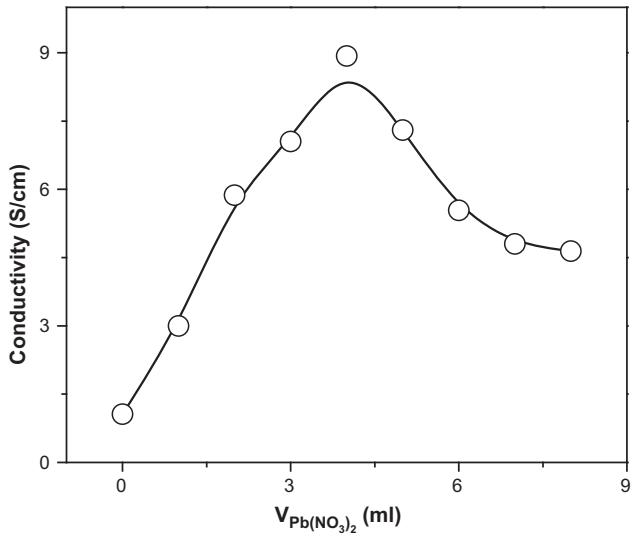

Fig. 13. The conductivity of Pb^{2+} vs. AA–AO (with equivalent ratio of AA and AO) in the solution (Table 3) (T = 298 K).

chlorobenzene, and n-hexane experiment revealed that CTAB-modified P(A-O)/AT displayed excellent selective adsorption to phenol among organic molecules. Therefore, phenol was chosen as the adsorption object.

3.3.1. *Effect of initial pH*

The effect of pH on adsorption of phenol was shown in Fig. 15. It was observed that the adsorption capacity plot resembled a hill

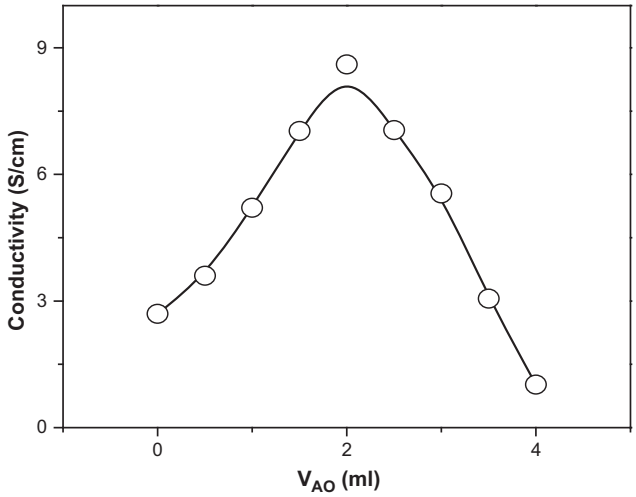

Fig. 14. The conductivity of Pb^{2+} vs. AA–AO (with different ratio of AA and AO) in the solution (Table 4).

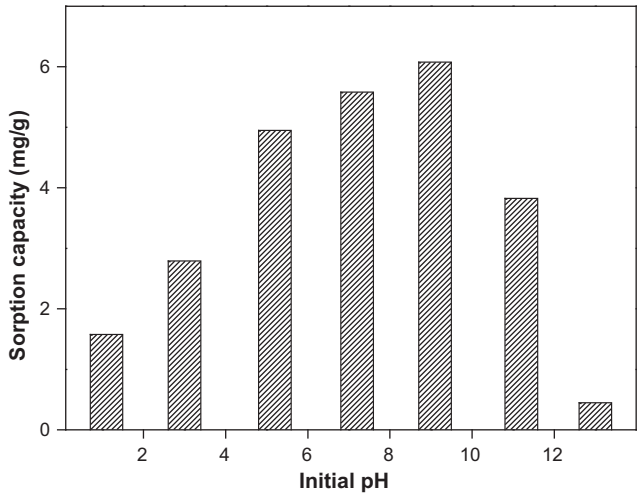

Fig. 15. Effect of initial pH on the adsorption of phenol.

with pH value change. The largest adsorption of phenol occurred at pH 9.0. The aim of introducing CTAB which has a hydrophobic group and positive charge was to attract phenol molecules in water. After the CTAB-modified P(A-O)/AT samples were shaked adequately under different pH values at 25 °C, the ammonia content was detected (Fig. 16). It could be seen the ammonia content was high in an acidic or strong alkalinic environment. However, at pH 9.0, the ammonia content was the lowest. The value of ammonia content reflected the amount of free CTAB in the solution, indicating that the lower the ammonia content was, the better CTAB combined with the P(A-O)/AT nano-adsorbent. The scheme in Fig. 17 showed

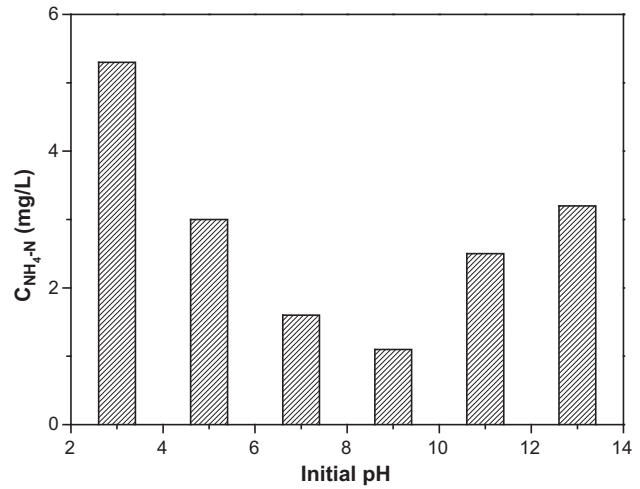

Fig. 16. Effect of initial pH on the amount adsorbed of ammonia (T = 25 °C, contact time = 24 h).

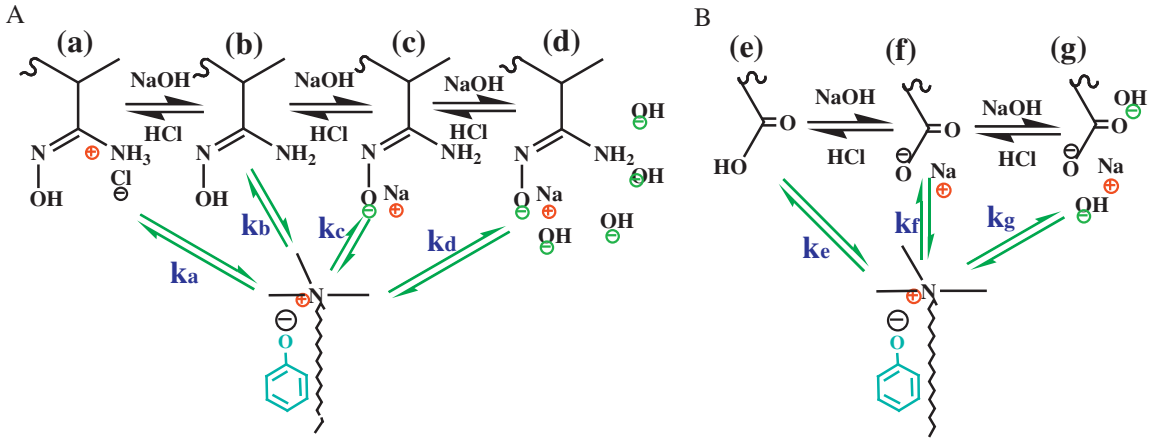

Fig. 17. Proposed schematic diagram for the complex formation between phenol, CTAB and AO(AA).

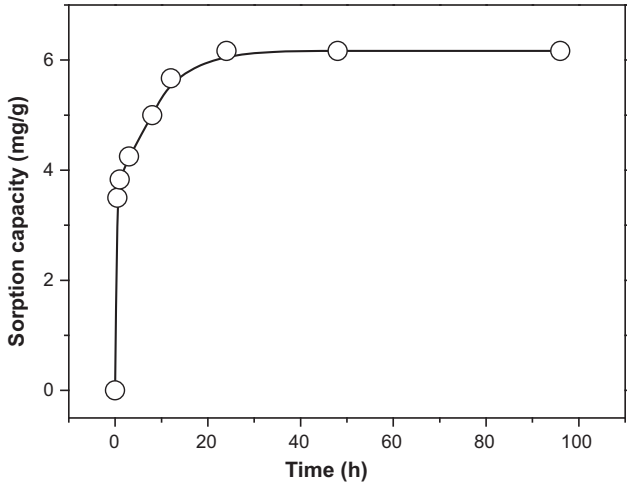

Fig. 18. Effect of contact time on the adsorption of phenol.

that CTAB combined with AO and AA at different pH values, which was a reversible process. At low pH value AO was at the state of (a) (Fig. 17). In this case, the combination of AO and CTAB was difficult. The reason was that protonation of the amide groups led to the positively charged molecules which rejected with positively charged CTAB. AO did not carry electrical charge (Fig. 17b) when the pH value was at the isoelectric point, which combined with CTAB relied on Van der Waals force under these conditions. With the increase of pH, the bonding force between negatively charged AO (Fig. 17c) and positively charged CTAB increased gradually. The increase of pH would reduce the effect of CTAB combining with the P(A-O)/AT when OH^- could compete with the combination of AO (Fig. 17d) with CTAB. AA was similar to AO in bonding with CTAB. Considering the different isoelectric points of AA and AO and complex solution conditions, pH 9 was the best pH value.

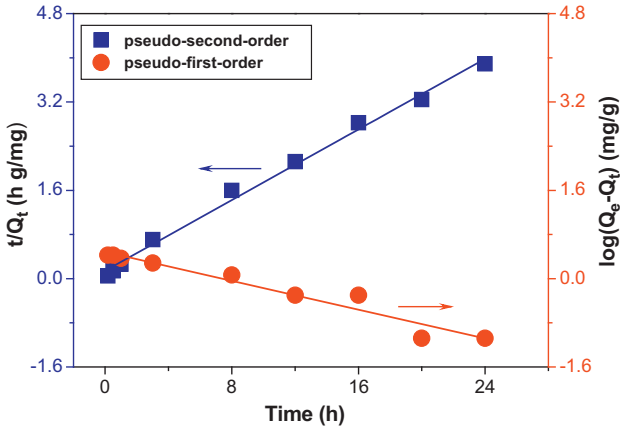

Fig. 19. The pseudo-first-order kinetics (a) and the pseudo-second-order kinetics (b) for the adsorption of Pb^{2+} onto P(A-O)/AT.

Table 5
Parameters of kinetic models of Pb^{2+} adsorption onto P(A-N)/AT and P(A-O)/AT.

Sample	Pseudo-first-order			Pseudo-second-order		
	Q_{e1} (mg/g)	K_1 (min^{-1})	R_1^2	Q_{e2} (mg/g)	K_2 (g/mg min)	R_2^2
P(A-O)/AT	3.039	0.1152	0.9409	6.252	0.2662	0.9934

3.3.2. Adsorption kinetics

The relationship between contact time and phenol uptake by the CTAB-modified P(A-O)/AT was presented in Fig. 18 at the initial phenol concentrations of 100 mg/l. The equilibrium time required for the adsorption of phenol was almost 20 h for the nanoparticles. However, to ensure equilibrium, the subsequent experiments were left for 96 h. It was also noted from these figures that the sorption process was divided into three regimes. The first regime was very fast characterized by rapid attachment of phenol to the surface of the sorbent. The second regime, which was slower due to the intra-particle diffusion, and the third regime where the sorption process was ceased indicating equilibrium. Compared with similar materials [45,46], the hybrid nano-adsorbent had obvious advantages whose adsorption capacity could achieve 6.25 mg/g.

It could be seen from Fig. 19 and Table 5, that the pseudo-second-order yielded a better fit than the pseudo-first-order by comparing the results of the correlation coefficient (R^2) values; the correlation coefficient were found to be 0.9934 and 0.9409. The main reason for this trend was the electrostatic interaction between adsorbent molecules (hybrid nano-adsorbent) and adsorbate (phenol). The behavior of Pb^{2+} sorption on CTAB-modified P(A-O)/AT was in agreement with chemical adsorption.

4. Conclusion

In this study, we synthesized a novel organic–inorganic hybrid nano-adsorbent (P(A-O)/AT) for the adsorption of metal ions and organic molecules. The adsorption removal of P(A-O)/AT for 120.0 mg/l Pb^{2+} achieved more than 96.6%, and the maximum removal capacity was 109.9 mg/g. In addition, adsorption kinetic

data were described by pseudo-second-order equation and the equilibrium data fitted very well with the Freundlich model. We researched the adsorption mechanism of Pb^{2+} onto P(A-O)/AT and speculated that the logical coordination ratio of the ligands was 1:1 (AO:AA). Meanwhile, CTAB-modified P(A-O)/AT had excellent adsorption properties for phenol and the adsorption amount achieved 6.2 mg/g. The adsorption of phenol was optimal at pH 9.0, and the adsorption kinetics of phenol by P(A-O)-CTAB/AT followed pseudo-second-order model. It was concluded that the organic–inorganic hybrid nano-adsorbent, P(A-O)/AT was a promising alternative adsorbent for rapidly removing Pb^{2+} and phenol from individual aqueous solutions.

Acknowledgements

The authors gratefully acknowledge financial supports from the National Major Specific Program of Science and Technology on Controlling and Administering of Water's Pollution (2008ZX07212-001-04), the Committee of Natural Science Foundation in China on National Training Fund for Person with Ability of Basic Subjects (J0730425) and Key Research Program of Gansu Province (2GS064-A52-036-02, GS022-A52-082). Thanks to Dr. Jie Mao for the mechanism discussion.

Appendix A. Supplementary data

Supplementary data associated with this article can be found, in the online version, at doi:10.1016/j.jhazmat.2010.12.057.

References

[1] X.G. Li, X.L. Ma, J. Sun, M.R. Huang, Powerful reactive sorption of silver(I) and mercury(II) onto poly(o-phenylenediamine) microparticles, Langmuir 25 (2009) 1675–1684.
[2] K.M. Popat, P.S. Anand, B.D. Dasare, Selective removal of fluoride ions from water by aluminum from of the aminomethylphosphonic acid type ion exchanger, React. Polym. 23 (1994) 23–32.
[3] N. Unlu, M. Ersoz, Adsorption characteristics of heavy metal ions onto a low cost biopolymeric sorbents from aqueous solution, J. Hazard. Mater. 136 (2006) 272–280.
[4] Q.S. Liu, T. Zheng, P. Wang, J.P. Jiang, N. Li, Adsorption isotherm, kinetic and mechanism studies of some substituted phenols on activated carbon fibers, Chem. Eng. J. 157 (2010) 348–356.
[5] S.K. Allen, C.W. Allen, Phenol concentrations in air and rain water samples collected near a wood preserving facility, Bull. Environ. Contam. Toxicol. 59 (1997) 702–709.
[6] N.N. Dutta, S. Brothakur, R. Baruah, A novel process for recovery of phenol from alkaline wastewater: laboratory study and predesign cost estimate, Water Environ. Res. 70 (1998) 4–9.
[7] X.W. Zeng, Y.G. Fan, G.L. Wu, C.H. Wang, R.F. Shi, Enhanced adsorption of phenol from water by a novel polar post-crosslinked polymeric adsorbent, J. Hazard. Mater. 169 (2009) 1022–1028.
[8] S.A. Boyd, S. Shaobia, J. Lee, M.M. Mortland, Pentachlorophenol sorption by organo-clays, Clay Clay Miner. 35 (1988) 125–130.
[9] M.C. Hermosin, P. Martín, J. Cornejo, Adsorption mechanisms of monobutyltin in clay, Miner. J. Environ. Sci. Technol. 27 (1993) 2606–2611.
[10] A. Demirbas, Heavy metal adsorption onto agro-based waste materials: a review, J. Hazard. Mater. 157 (2008) 220–229.
[11] P. Menoud, L. Cavin, A. Renken, Modelling of heavy metals adsorption to a chelating resin in a fluidized bed reactor, Chem. Eng. Process. 37 (1998) 89–101.
[12] O. Abollino, M. Aceto, M. Malandrino, C. Sarzanini, E. Mentasti, Adsorption of heavy metals on Na-montmorillonite. Effect of pH and organic substances, Water Res. 37 (2003) 1619–1627.
[13] M.O. Corapcioglu, C.P. Huang, The adsorption of heavy metals onto hydrous activated carbon, Water Res. 21 (1987) 1031–1044.
[14] K. Kadirvelu, K. Thamaraiselvi, C. Namasivayam, Removal of heavy metals from industrial wastewaters by adsorption onto activated carbon prepared from an agricultural solid waste, Bioresour. Technol. 76 (2001) 63–65.
[15] I.I. Salame, T.J. Bandosz, Role of surface chemistry in adsorption of phenol on activated carbons, J. Colloid Interface Sci. 264 (2003) 307–312.
[16] B.H. Hameed, A.A. Rahman, Removal of phenol from aqueous solutions by adsorption onto activated carbon prepared from biomass material, J. Hazard. Mater. 160 (2008) 576–581.
[17] E. Malkoc, Y. Nuhoglu, Investigations of nickel (II) removal from aqueous solutions using tea factory waste, J. Hazard. Mater. 127 (2005) 120–128.
[18] A. Kara, B. Acemioglu, M. Hakki, M. Cebe, Adsorption of Cr (III), Ni(II), Zn(II), Co(II) ions onto phenolated wood resin, J. Appl. Polym. Sci. 101 (2006) 2838–2846.
[19] K.G. Bhattacharyya, S.S. Gupta, Adsorption of chromium (VI) from water by clays, Ind. Eng. Chem. Res. 45 (2006) 7232–7340.
[20] M.A. Andeson, Removal of MTBE and other organic contaminates from water by sorption to high silica zeolites, Environ. Sci. Technol. 34 (2000) 725–727.
[21] S.R. Shukla, R.S. Pai, Adsorption of Cu(II), Ni(II) and Zn(II) on modified jute fibres, Bioresour. Technol. 96 (2005) 1430–1438.
[22] S.H. Huang, D.H. Chen, Rapid removal of heavy metal cations and anions from aqueous solutions by an amino-functionalized magnetic nano-adsorbent, J. Hazard. Mater. 163 (2009) 174–179.
[23] N. Boujelben, J. Bouzida, Z. Elouear, Adsorption of nickel and copper onto natural iron oxide-coated sand from aqueous solutions: study in single and binary systems, J. Hazard. Mater. 163 (2009) 376–382.
[24] Y.S. Ho, T.H. Chiang, Y.M. Hsueh, Removal of basic dye from aqueous solution using tree fern as a biosorbent, Process Biochem. 40 (2005) 119–124.
[25] B.S. Inbaraj, J.S. Wang, J.F. Lu, F.Y. Siao, B.H. Chen, Adsorption of toxic mercury (II) by an extracellular biopolymer poly(γ-glutamic acid), Bioresour. Technol. 100 (2009) 200–207.
[26] Q. Wu, P. Tian, Adsorption of Cu^{2+} ions with poly(N-isopropylacrylamide-comethacrylic acid), J. Appl. Polym. Sci. 109 (2008) 3470–3476.
[27] L.Q. Yang, Y.F. Li, Preparation and adsorption performance of a novel bipolar PS-EDTA resin in aqueous phase, J. Hazard. Mater. 180 (2010) 98–105.
[28] S. Zhu, N. Yang, D. Zhang, Poly(N,N-dimethylaminoethylmethacrylate) modification of active carbon for copper ions removal, Mater. Chem. Phys. 377 (2009) 784–789.
[29] J.H. Huang, Adsorption properties of a microporous and mesoporous hypercrosslinked polymeric adsorbent functionalized with phenoxy groups for phenol in aqueous solution, J. Colloid Interface Sci. 339 (2009) 296–301.
[30] M.C. Xu, Y. Zhou, J.H. Huang, Adsorption behaviors of three polymeric adsorbents with amide groups for phenol in aqueous solution, J. Colloid Interface Sci. 32 (2008) 9–14.
[31] X. Liu, H. Chen, Synthesis of porous acrylonitrile/methyl acrylate copolymer beads by suspended emulsion polymerization and their adsorption properties after amidoximation, J. Hazard. Mater. 175 (2010) 1014–1021.
[32] A. Nilchi, A.A. Babalou, R. Rafiee, H. Sid Kalal, Adsorption properties of amidoxime resins for separation of metal ions from aqueous systems, React. Funct. Polym. 68 (2008) 1665–1670.
[33] M.J. Zohuriaan-Mehr, A. Pourjavadi, M. Salehi-Rad, Modified CMC. 2. Novel carboxymethyl cellulose-based poly(amidoxime) chelating resin with high metal sorption capacity, React. Funct. Polym. 61 (2004) 23–31.
[34] N.M. El-Sawy, E.A. Hegazy, A. El-Hag Ali, M.S. Abdel Motlab, A. Awadallah-F, Physicochemical study of radiation-grafted LDPE copolymer and its use in metal ions adsorption, Nucl. Instrum. Methods B 264 (2007) 227–234.
[35] P. Vindevoghel, A. Gugot, Suspended emulsion copolymerization of acrylonitrile and methyl acrylate, Polym. React. Eng. 3 (1995) 23–42.
[36] Y. Xue, H. Houa, S. Zhu, Competitive adsorption of copper(II), cadmium(II), lead(II) and zinc(II) onto basic oxygen furnace slag, J. Hazard. Mater. 162 (2009) 391–401.
[37] S.L. Sun, L. Wang, A.Q. Wang, Adsorption properties of crosslinked carboxymethyl-chitosan resin with Pb(II) as template ions, J. Hazard. Mater. B136 (2006) 930–937.
[38] O. Moradi, M. Aghaieb, K. Zarea, M. Monajjemi, H. Aghaie, The study of adsorption characteristics Cu^{2+} and Pb^{2+} ions onto PHEMA and P(MMA-HEMA) surfaces from aqueous single solution, J. Hazard. Mater. 170 (2009) 673–679.
[39] M. Kawaguchi, A. Takahashi, Polymer adsorption at solid–liquid interfaces, Adv. Colloid Interface Sci. 37 (1992) 219–317.
[40] E. Guibal, C. Milot, J.M. Tobin, Metal–anion sorption by chitosan beads: equilibrium and kinetic studies, Ind. Eng. Chem. Res. 37 (1998) 1454–1463.
[41] P. Baskaralingam, M. Pulikesi, D. Elango, V. Ramamurthi, S. Sivanesan, Adsorption of acid dye onto organ obentonite, J. Hazard. Mater. 128 (2006) 138–144.
[42] L. Jin, R.B. Bai, Mechanisms of lead adsorption on chitosan/PVA hydrogel beads, Langmuir 18 (2002) 9765–9770.
[43] Z.J. Yu, E.T. Kang, K.G. Neoh, Amidoximation of the acrylonitrile polymer grafted on poly(tetrafluoroethylene-co-hexafluoropropylene) films and its relevance to the electroless plating of copper, Langmuir 18 (2002) 10221–10230.
[44] X.M. Yang, G.Y. Liu, H.C. Li, Y. Zhang, D.D. Song, C.M. Li, R. Wang, B. Liu, W. Liang, Y.K. Jing, G.S. Zhao, Novel oxadiazole analogues derived from ethacrynic acid: design, synthesis, and structure-activity relationships in inhibiting the activity of glutathione S-transferase P1-1 and cancer cell proliferation, J. Med. Chem. 53 (2010) 1015–1022.
[45] A. Tor, Y. Cengeloglu, M.E. Aydin, M. Ersoz, Removal of phenol from aqueous phase by using neutralized red mud, J. Colloid Interface Sci. 300 (2006) 498–503.
[46] J.H. Huang, X.G. Wang, Q.Z. Jin, Y.F. Liu, Y. Wang, Removal of phenol from aqueous solution by adsorption onto OTMAC-modified attapulgite, J. Environ. Manage. 84 (2007) 229–236.